Supporting Information for *Microcoining ripples in metal foils*

Greg C. Randall[a,*], Jinesh Dahal[c], James Vecchio[a], Shashank Agarwal[b], Rounak Mehta[b], G. Ravichandran[b], Aaron Stebner[c]

[a] *General Atomics, 3550 General Atomics Ct., San Diego, CA 92121*
[b] *Caltech, 1200 E California Blvd., Pasadena, CA 91125*
[c] *Colorado School of Mines, 1500 Illinois St., Golden, CO 80401*

S1. Kudo's upper bound method and calculations

Upper-bound theory is a simplified metal forming calculation technique that predicts upper bounds on the pressures required for an ideal rigid-plastic deformation. General aspects and derivations are presented in textbooks, e.g. Hosford Ch. 8 [1] or Avitzur Ch. 5 [2]. As depicted in Fig. S1 (a) and (b) in examples to be discussed below, Kudo [3] showed that complex geometric plane strain forming problems could be approximated by splitting the plastic region into i unit rectangles so that:

$$\frac{p_m}{Y} = \frac{\sum_i e_i A_i u_i}{Au} \tag{S1}$$

where A is the area under load, u is the load velocity, A_i is the compressed surface area of each unit rectangle, u_i is that surface's velocity, and e_i is the dimensionless energy dissipation rate of each unit rectangle. Specifically, $e_i = \int_{S_i} u_{S_i} dS_i/(2A_i u_i)$ where S_i are the surfaces of velocity discontinuity (u_{S_i}) bordering or within the unit rectangle i. Kudo tabulated e_i for unit rectangles of varying aspect ratio and frictional boundary conditions in Ref. [3] Table I. In order to use Eq. S1, one must understand Kudo's shorthand notation for the unit rectangle (of dimension $h \times w$) to order and label its four boundaries as either s meaning smooth or r meaning rough. Ref. [3] is required for the details of the unit rectangle and boundary condition shorthand notation (e.g. *ssrr(i)*) which we summarize in Fig. S1 (c) and will employ in the following. In addition to the boundary conditions, each e_i will be a function of the unit rectangle aspect ratio ($a_i = h/w$) and number of self-similar slip line fields n_i within the unit rectangle. The upper bound solution method involves minimizing the upper bound forming load p_m calculated in Eq. S1 with respect to a unit rectangle dimension and n_i. Despite the approximations involved, this method has been shown to sufficiently match experimental and slip-line forming loads [3].

S1.1. Compression of a thin metal on smooth and rough surfaces

When a metal foil is compressed between flat rough dies (Fig. S1 (a)), the part can be divided into two symmetric unit rectangles with a boundary condition *srrr(i)*. The solution can be obtained looking at one

*Corresponding author. Tel: (858) 455-3000 Fax: (858) 455-3181
Email address: randall@fusion.gat.com (Greg C. Randall)

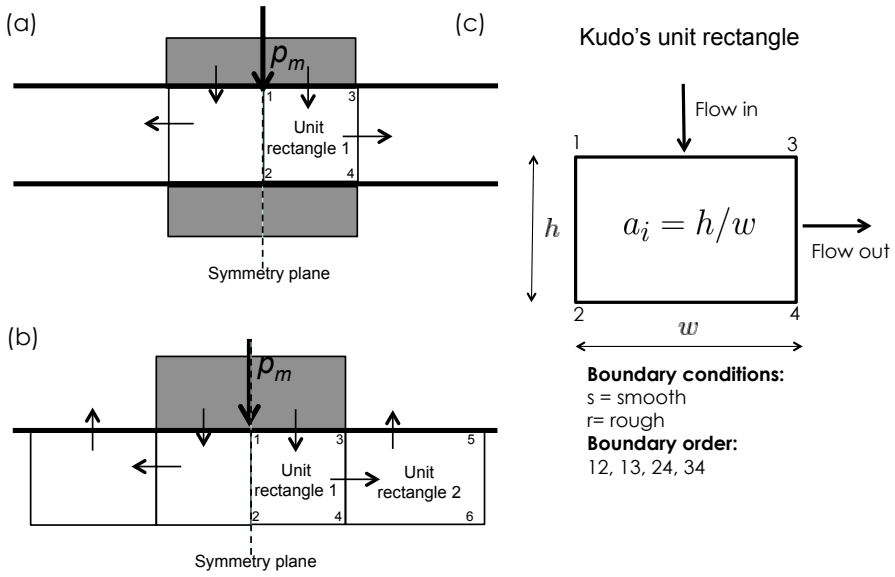

Figure S1: (a) Kudo's unit rectangles for compression of a foil between plates (b) Kudo's unit rectangles for indentation. (c) Kudo's unit rectangle geometry and boundary condition notation.

side of the axis of symmetry which maps as a single unit rectangle with $a = t/R_{die}$. Using Ref. [3] Table I to find e for a *srrr(i)* unit rectangle, the indentation pressure in Eq. S1 is:

$$\frac{p_m}{Y} = \left(n - \frac{1}{2}\right)\frac{t}{2R_{die}} + \frac{(n+\frac{1}{2})}{(4n-1)}\frac{2R_{die}}{t} + \frac{t}{4R_{die}} \tag{S2}$$

where n is the number of self-similar cells within the unit rectangle which depends on the die and workpiece geometry. Performing the minimization $\partial p_m/\partial n = 0$ gives $n = 1/4 + R_{die}\sqrt{3}/(2t)$ so that:

$$\frac{p_m}{Y} = \frac{\sqrt{3}}{2} + \frac{t}{8R_{die}} + \frac{R_{die}}{2t} \tag{S3}$$

The load grows linearly with decreasing thickness to die size ratio, so to compress very thin foils, e.g. for a width/thickness ratio ~ 100, pressures greater than $10Y$ would be required. For ideally smooth die surfaces, a similar analysis gives $p_m/Y = 1$. The situation of one rough and one smooth die can be worked similarly and results in intermediate loads. Similarly, a potentially more realistic Coulomb friction boundary could be approximated as a fraction of this rough die load in Eq. S3.

For metals thick enough that $t/(2R_{die}) \gtrsim 8$, the slip line field changes to an indentation field [3, 4]. The frictionless die indentation problem is solved in Ref. [3] in the same manner we just outlined with two unit rectangles on one half of the symmetry plane, the first with boundaries *ssrr(i)* and the second with *rrr* (Fig. S1 (b)). For a frictionless die, $p_m/Y = \sqrt{7} = 2.65$, which is very close to values obtained with more detailed slip line fields ($p/Y = 1 + \pi/2 = 2.57$) [4]. In the case of a rough die, the first unit rectangle is now *srrr(i)*, and $p_m/Y = \sqrt{2} + \sqrt{7}/2 = 2.74$. In general, die friction is not considered a significant contribution

to indentation loads.

S1.2. Frictionless inverse extrusion: closed die coining

The frictionless inverse extrusion problem (see Fig. 3 (a) of the main paper) can be solved with two unit rectangles right of the die symmetry axis, the first with boundaries *ssrr(i)* and the second with *rrs*, where $a_1 = 2G/(\alpha\lambda)$ and $a_2 = \lambda(1-\alpha)/(2G)$ and G is the depth of the plastic deformation zone. With $u_1 = u$ and $u_2 = u\alpha\lambda/(2G)$ by continuity, and $a \sim \lambda$, $a_1 \sim \alpha\lambda/2$, and $a_2 \sim G$, the upper bound indentation pressure in Eq. S1 is:

$$\frac{p_m}{Y} = \alpha(e_1 + e_2) \tag{S4}$$

where e_1 is the dimensionless dissipation rate from unit rectangle 1 and e_2 is the dimensionless dissipation rate from unit rectangle 2 found in Kudo's Table I [3]. Given the small ripple amplitude to wavelength ratio ($A/\lambda \ll 1$) in this analysis, we assume unit rectangles with aspect ratios $a_i < 1$, which can be verified at the end of the upper bound solution. Specifically, this requires $G < \alpha\lambda$ and $G > (1-\alpha)\lambda/2$. The dimensionless dissipation rates are:

$$\begin{aligned} e_1 =& n_1 a_1 + \frac{n_1 + \frac{3}{4}}{4n_1}\frac{1}{a_1} \\ e_2 =& n_2 a_2 + \frac{n_2 + \frac{3}{4}}{4n_2}\frac{1}{a_2} \end{aligned} \tag{S5}$$

Solving for n_1 and n_2 by minimizing the upper bound pressure, i.e. $\partial p_m/\partial n_1 = 0$ and $\partial p_m/\partial n_2 = 0$, gives $n_1 = \sqrt{3}/(4a_1)$ and $n_2 = \sqrt{3}/(4a_2)$. Plugging these into Eq. S5 and minimizing the upper bound pressure in Eq. S4 with respect to G, gives $G = \lambda\sqrt{\alpha(1-\alpha)}/2$, which satisfies the initial assumptions for unit rectangle geometry. Inserting these expressions for a_1, a_2, and G into Eq. S4 gives:

$$\frac{p_m}{Y} = \sqrt{3}\alpha + \frac{\alpha}{2}\sqrt{\frac{\alpha}{1-\alpha}} \tag{S6}$$

The final term grows sharply as $\alpha \to 1$ and is due to the shrinking plastic region causing the growing internal friction (e.g. more n_i in upper bound unit rectangles).

S1.3. Inverse extrusion with friction: closed die coining

The inverse extrusion problem with sticking friction can be solved with two unit rectangles right of the die symmetry axis, the first now with boundaries *srrr(i)* and the second with *rrs*. Note the only difference from the frictionless die inverse extrusion problem is the boundary where the die touches the metal is now r instead of s. The dimensionless dissipation rates e_1 and e_2 are found in Kudo's Table I [3]:

$$\begin{aligned} e_1 =& \Big(n_1 - \frac{1}{2}\Big)\frac{a_1}{2} + \frac{(n_1 + \frac{1}{2})}{(4n_1 - 1)}\frac{2}{a_1} + \frac{a_1}{4} \\ e_2 =& n_2 a_2 + \frac{(n_2 + \frac{3}{4})}{4n_2}\frac{1}{a_2} \end{aligned} \tag{S7}$$

Solving for n_1 and n_2 by minimizing the upper bound pressure, i.e. $\partial p_m/\partial n_1 = 0$ and $\partial p_m/\partial n_2 = 0$, gives $n_1 = 1/4 + \sqrt{3}/(2a_1)$ and $n_2 = \sqrt{3}/(4a_2)$. Using $a_1 = 2G/(\alpha\lambda)$ and $a_2 = \lambda(1-\alpha)/(2G)$ and minimizing the upper bound pressure with respect to G gives $G = \alpha\lambda\sqrt{\frac{(1-\alpha)}{(1+\alpha)}}$. Using these expressions for n_1, n_2, and G gives:

$$\frac{p_m}{2k} = \sqrt{3}\alpha + \frac{\alpha}{2}\sqrt{\frac{1+\alpha}{1-\alpha}} \tag{S8}$$

S1.4. Open die coining

We assume a neutral plane exists in the metal dividing sideways upsetting flow from the vertical coining flow and determine what load is now required to fill the die grooves. The analysis is very similar to the above with the changes that 1) the die filling on the λ length scale is one-directional with flow moving outwards from the center of the die and 2) the lower boundary of the coining region, at the neutral plane, is now frictionless.

As above, the problem can be solved with two unit rectangles, the first with boundaries *rssr(i)* and the second with *srr*. These are shown in Figure 3 (b) of the main paper. The upper bound indentation pressure in Eq. S1 is:

$$\frac{p_m}{Y} = \alpha(e_1 + e_2) \tag{S9}$$

Initial analysis pointed to a very thin plastic zone above the neutral plane, i.e. $\partial p_m/\partial G \to 0$ as $G \to 0$. Consequently the unit rectangles are assumed to have aspect ratios $a_1 < 1$ and $a_2 > 1$. The dimensionless dissipation rates are calculated in Kudo's Table I [3] as:

$$\begin{aligned} e_1 =& n_1 a_1 + \frac{1}{4 n_1 a_1} \\ e_2 =& \frac{n_2}{a_2} + \frac{a_2}{4 n_2} \end{aligned} \tag{S10}$$

where $a_1 = G/(\alpha\lambda)$, $a_2 = \lambda(1-\alpha)/G$, and the depth between the surface and the neutral plane is G. Solving for n_i by minimizing the upper bound pressure, i.e. $\partial p_m/\partial n_i = 0$ gives $n_1 = 1/(2a_1)$ and $n_2 = (1-\alpha)\lambda/(2G)$. Therefore, $e_1 = e_2 = 1$ and the open die load is:

$$\frac{p_m}{Y} = 2\alpha \tag{S11}$$

S2. Strain calculation for closed die coining

Given the small ripple amplitude to wavelength ratio ($A/\lambda \ll 1$), a gross estimate for the strain in coining is $\alpha - 1/2$, which is the compression in unit rectangle 2 divided by the plastic volume at the start of the inverse extrusion portion of coining. Consequently we would expect compressive strains on the order of 0.5 at full patterning. However, we can use the upper bound solution to attempt a more detailed, yet still approximate, solution for the strain.

First, we assume strain can be decomposed into plastic strain during the initial contact (before ripple plastic regions begin to overlap, i.e. $\bar{\varepsilon}_0$ at $\alpha = 0.5$) and plastic strain during the extrusion part of coining ($\bar{\varepsilon}_p(\alpha)$) so that $\bar{\varepsilon} = \bar{\varepsilon}_0 + \bar{\varepsilon}_p(\alpha)$. A strain increment analysis gives $d\bar{\varepsilon}_p = |\delta l/l| = d\alpha'/(1-\alpha')$ where we use the incremental fractional area increase $d\alpha'$ to parametrize the coining evolution. This is the compressive plane strain experienced by an unpatterned surface element of length $l = \lambda - \alpha\lambda$ incrementally forming into the die ripple cavity [5]. Integrating from $\alpha' = 0.5$ to α gives the plastic strain at each stage of the extrusion part of coining: $\bar{\varepsilon}_p(\alpha) = \ln(1/(2-2\alpha))$. We will simply assume $\bar{\varepsilon}_0 = 0.08$ during the initial stage of coining, which is supported by simulation work [6] and also analogous to indentation before the deformation zones of neighboring ripples begin to interact. In order to calculate representative strain $\varepsilon_r(\alpha)$, we compute a plastic volume average of $\bar{\varepsilon}$ since the upper bound solutions solve for the depth of the plastic region $G(\alpha)$. We can parametrize the strained plastic volume per unit thickness with α as $V(\alpha) = G(\alpha)(1-\alpha)\lambda/2$; this is volume per unit thickness of unit rectangle 2 in our upper bound solution at each coining stage α. Using $G(\alpha) = \lambda\sqrt{\alpha(1-\alpha)}/2$ and $G_0 = G(0.5) = \lambda/4$, from the smooth die upper bound model, we find the representative strain at each stage of patterning progression:

$$\begin{aligned}
\varepsilon_r(\alpha) &= \frac{2}{G_0\lambda}\int \bar{\varepsilon} dV = \bar{\varepsilon}_0 + \frac{2}{G_0\lambda}\int_{1/2}^{\alpha} \bar{\varepsilon}_p(\alpha')\frac{dV}{d\alpha'}d\alpha' \\
&= \bar{\varepsilon}_0 + \frac{8}{\lambda^2}\int_{1/2}^{\alpha} \ln\frac{1}{2(1-\alpha')}\left(\frac{\lambda^2}{8}\left(\sqrt{\frac{1-\alpha'}{\alpha'}}(1-4\alpha')\right)\right)d\alpha' \\
&= \bar{\varepsilon}_0 + \int_{1/2}^{\alpha} \ln\frac{1}{2(1-\alpha')}\left(\sqrt{\frac{1-\alpha'}{\alpha'}}(1-4\alpha')\right)d\alpha'
\end{aligned} \tag{S12}$$

The same analysis can be performed using $G(\alpha)$ from the rough closed die model, and both results are plotted in Fig. 4(a) of the main paper. The representative strain approaches $\varepsilon_r = 0.5$ at full patterning in both cases.

S3. Simulation settings

Workpiece meshing was performed using 8-node linear brick, reduced integration, hourglass control hexagonal elements (Abaqus type C3D8R) close to the die and tetrahedral elements (C3D10M) in the region away from the die with lower strain gradients. A finer mesh was used near the regions where trough/crest of the sinusoidal profile is transferred for increased fidelity in the region of interest. 25 nodes were seeded over each 50 μm wavelength of the sinusoids with a biasing of 5 towards the crest and trough. In attempts with fewer seeds, incomplete tracing of the profile was observed. The die was modeled with rigid elements (R3D4). For computational efficiency, a quarter assembly with mass scaling 50 is simulated and symmetry boundary conditions are used on the sectioned surfaces.

Simulations were performed under both displacement and load control. Under displacement control, the rigid die was given a constant velocity keeping the workpiece support stationary. The load was applied in a smooth step polynomial with the first and second time derivatives equal to zero at the beginning and end of

the time interval. The simulation time had a lower limit in the fundamental natural mode of the workpiece as dynamic response of the material was neglected. This satisfied the Courant Condition and we ensured the simulation was quasi-static. As an additional check of the time step, we ensured that the kinetic energy was a small fraction (less than 1%) of the internal energy. Mesh and energy simulation studies were performed for validation. In the mesh study, various models with elements from ∼40,000-150,000 were studied to verify no excessive distortion in the elements close to die and hourglass effect was absent in the under the die. In the energy study, since mass scaling was applied on the explicit method, various simulations were carried out to minimize the kinetic energy. The model was optimized by running various simulations with increasing time step and decreasing mass scaling to reduce the inertial effect.

S4. Material properties and microhardness testing

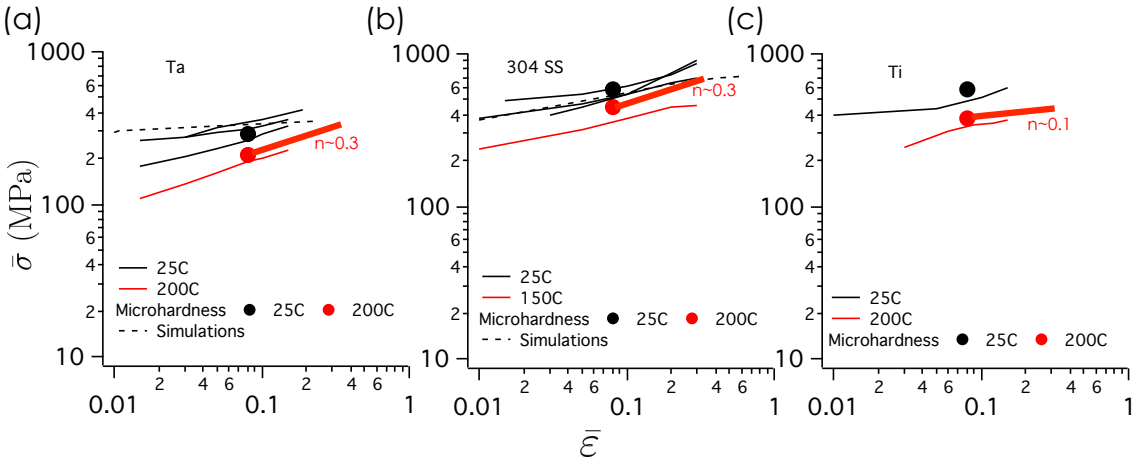

Figure S2: Microhardness and stress-strain ($\dot{\varepsilon} < 10^{-3}s^{-1}$) properties of (a) Ta, (b) 304SS, and (c) Ti. Room temperature values are in black while red indicates $\sim 200°$C. Thick red lines are superimposed to guide the eye to the expected regions of $\bar{\sigma}(\bar{\varepsilon})$ assumed in our thin foil (effectively closed die) coining model. The dashed lines in the Ta and SS304 plots show the material models used in our simulations.

References

[1] W. F. Hosford, R. M. Caddell, Metal Forming: Mechanics and Metallurgy, PTR Prentice Hall: New Jersey, 1993.

[2] B. Avitzur, Metal Forming: Process and Analysis, McGraw-Hill: New York, 1968.

[3] H. Kudo, An upper-bound approach to plane-strain forging and extrusion - i., Int. J. Mech. Sci. 1 (1960) 57–83.

[4] R. Hill, The Mathematical Theory of Plasticity, Oxford University Press: London, 1956.

[5] W. A. M. Brekelmans, L. H. G. Mulders, J. A. H. Ramaekers, The coining process: analytical simulations evaluated, CIRP Ann. 37 (1988) 235–238.

[6] H. Ike, A. Makinouchi, Effect of lateral tension and compression on plane strain flattening processes of surface asperities lying over a plastically deformable bulk, Wear 140 (1990) 17–38.